Computer-simulated schlieren optics

Gernot Decker, R. Deutsch, W. Kies, and J. Rybach

Computer-simulated schlieren pictures are used to interpret and quantitatively analyze schlieren pictures taken from a fast varying plasma with axial symmetry. Structurized angular distributions of deflected rays are obtained from a ray tracing simulation, the characteristics of which are related to density, density gradients, and dimensions of the plasma. Angular distributions are transformed into intensity distributions using the optical data of a typical schlieren system. Ranges of the plasma parameters density, density gradients, and dimensions are given. As an example the method is applied to the compression phase of a fast high voltage plasma focus.

I. Introduction

Schlieren methods are often used to get information about density gradients in various plasma experiments.[1,2] The availability of subnanosecond laser pulses now also allows analysis of the temporal evolution of fast varying plasmas with this technique.[3]

Quantitative evaluation of such schlieren pictures, however, is straightforward only for plane geometries whereas for plasmas with axial symmetry (e.g., θ, Z pinch, or plasma focus) or even more complicated ones (like tokamak) one had to put up with qualitative information or mere aesthetics. Quantitative results derived from an Abel inversion[4–6] are uncertain because of the ambiguity of the deflection angle vs the impact parameter. For definite results one had to determine this dependence experimentally which seems impossible in view of the many parameters involved.

Therefore computer simulations were made to quantitatively analyze schlieren pictures of plasmas with axial symmetry. Although our efforts were especially focused on a fast varying focus plasma, this ray tracing method is applicable to any system of axial symmetry.

Reducing the optical problem to the motion of simulating particles in a force field, a formalism is developed that is applied to different density profiles in two steps: first, calculating angular distributions, second, deriving simple formulas that visualize the dependence of characteristic peaks of these distributions on certain parameters of the density profile.

The dark-field schlieren method is used to appropriately transform these structurized distributions into intensity distributions (simulated schlieren pictures). Accessible parameter ranges for density, gradients, and radii of the plasma and approximation formulas are derived from intensity distributions.

As a numerical example the method is used to evaluate schlieren pictures taken at the fast, high voltage plasma focus SPEED 1.[7]

II. Theoretical Basis of the Simulation

Density gradients are supposed to satisfy the condition

$$\frac{1}{n_e}\,|\mathrm{grad} n_e| \ll \frac{1}{\lambda}, \tag{1}$$

where n_e is the electron density and λ is the wavelength of the laser light. In this case the methods of geometrical optics can be used.[4,5] Starting from the eikonal equation

$$(\nabla L)^2 = n^2(x,y,z) \tag{2}$$

and comparing it with the Hamilton-Jacobi equation

$$(\nabla S)^2 = 2m[E - U(x,y,z)] \tag{3}$$

(where L, S, m, and E are the optical path, the Hamilton-Jacobi function, the mass, and the energy of the simulating particles, respectively), the equivalent potential $U(x,y,z)$ of the hypothetical field in which the simulating particles move can be expressed through the refractive index $n(x,y,z)$ as a function of the spatial coordinates. The function

$$f(x,y,z) = 1 - n^2(x,y,z) \tag{4}$$

When this work was done all authors were with Universität Düsseldorf, Physikalisches Institut I, D-4000 Düsseldorf, Federal Republic of Germany; J. Rybach is now with Philips Kommunikations Industrie AG, Unternehmensbereich F & G, D-5000 Köln 80, Federal Republic of Germany.

Received 9 July 1984.
0003-6935/85/060823-06$02.00/0.

is used instead of $n(x,y,z)$ because of its direct connection with the density profile.

In a fully ionized plasma we have

$$f(x,y,z) = \frac{\omega_p^2}{\omega^2} = A\lambda^2 n_e(x,y,z), \tag{5}$$

where ω_p is the electron plasma frequency, ω and λ are the frequency and wavelength (in cm) of the laser light, n_e is the electron density in cm^{-3}, and $A = 8.9 \times 10^{-14}$ cm.

In this way the whole optical problem is reduced to a study of the motion of simulating particles in a force field determined by the density profile of the plasma and the characteristics of the optical system. An easy and intuitive way to trace the rays is to reduce the whole mechanical problem to the solution of the equation

$$\frac{d^2\mathbf{r}}{d\tau^2} = -\frac{1}{2}\,\mathrm{grad}f \tag{6}$$

with the initial conditions

$$\left.\frac{d\mathbf{r}}{d\tau}\right|_{\tau=0} = n(\mathbf{r}_0)\mathbf{e} \text{ and } \mathbf{r}|_{\tau=0} = \mathbf{r}_0$$

for different density profiles ($\mathbf{r}_0$ and $\mathbf{e}$ characterize the starting point and the direction, respectively, of the simulating particle).

III. Plasmas with Axial Symmetry

A. Density Profiles

Dynamic pinches produce axially symmetric current-carrying plasma layers (hollow cylinders) that are finally compressed to full cylinders by the magnetic field. Therefore, a density profile

$$n_e = \frac{N_0}{2} + \frac{N - N_0}{2}\tanh\frac{r - r_1}{d_1} - \frac{N}{2}\tanh\frac{r - r_2}{d_2} \tag{7}$$

is chosen which includes both cases. (N denotes maximum electron density inside the layer, N_0 is the density in the region surrounded by the layer, d_1 and d_2 are the characteristic widths of the inner and outer density gradient regions, r_1 is the inner radius, and r_2 is the outer radius of the plasma layer). [Other types of profile with similar slopes lead to almost the same results because the tails (low gradient regions) do not contribute much to light deflection and small deflection angles do not contribute to the schlieren picture at all.]

The primary interest of this paper is to study the behavior of the plasma layer during compression, but the *ansatz* can as well be applied to the "full cylinder" to which case the calculations have been restricted so far.[4–6]

Figure 1 shows a plot of normalized density profile and gradient, respectively.

B. Angular Distributions

Typically 5000 simulating particles (moving initially parallel) are made to interact with the axially symmetric plasma layer (dashed lines) as shown in Fig. 2. The trajectories of these particles that represent the optical rays are determined by numerical integration of Eq. (6)

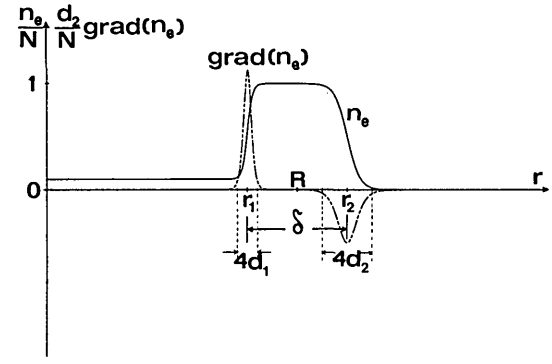

Fig. 1. General density profile used for computer simulations.

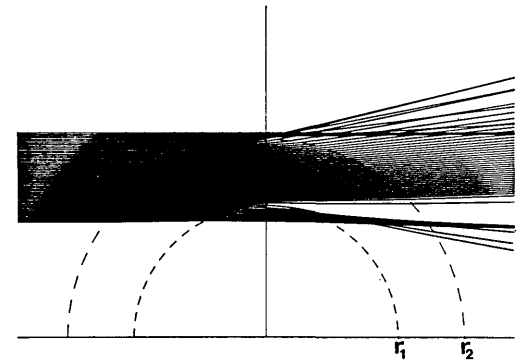

Fig. 2. Ray tracing through a plasma layer of axial symmetry: $N = 10^{20}$ cm^{-3}, $N_0 = 10^{18}$ cm^{-3}, $r_1 = 8$ mm, $r_2 = 12$ mm, $d_1 = d_2 = 0.1$ mm, $\lambda = 600$ nm.

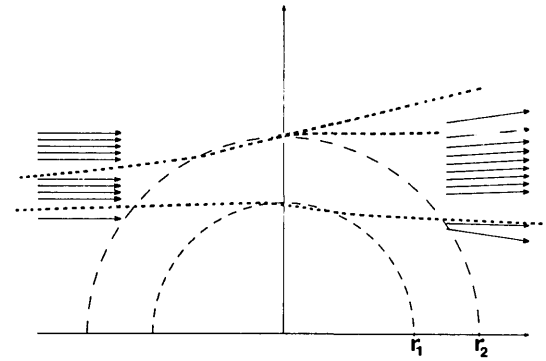

Fig. 3. Caustics caused by a plasma layer of axial symmetry: $N = 10^{20}$ cm^{-3}, $N_0 = 10^{18}$ cm^{-3}, $r_1 = 8$ mm, $r_2 = 12$ mm, $d_1 = d_2 = 0.1$ mm, $\lambda = 600$ nm.

using the density profile of Eq. (7) with the parameter values given in Fig. 2.

Unfortunately, the rays are deflected in such a way that no plane (e.g., the midplane of the plasma) exists that could be considered as the object from which the rays originate and which could be imaged by the schlieren system. Rather, there are causticlike extended envelopes (dotted lines) of intersection points as visualized in Fig. 3.

Figure 4 shows the angular distribution of the rays after interaction with the plasma layer for the given parameter values. Three pronounced peaks appear in

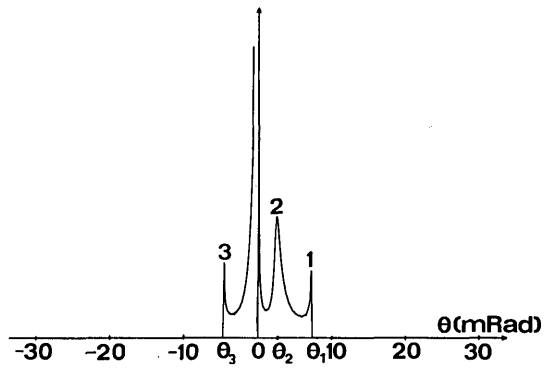

Fig. 4. Angular distribution of incident parallel rays after deflection in a plasma layer of axial symmetry: $N = 2 \times 10^{18}$ cm^{-3}, $N_0 = 10^{17}$ cm^{-3}, $r_1 = 9.75$ mm, $r_2 = 10.25$ mm, $d_1 = d_2 = 0.05$ mm, $\lambda = 600$ nm.

addition to the large number of undeflected rays that cause the very intense central maximum: peak 1 is due to the outer gradient region, peak 2 stems mainly from the region of maximum density, whereas peak 3 is predominantly caused by the inner gradient region of the plasma layer.

C. Approximation Formulas

These structurized angular distributions allow approximation formulas for the peaks described above to be derived.

Since the deflection angle is proportional to both the density gradient (N/d_2) and the interaction path length $[(r_2 d_2)^{1/2}]$, the maximum angle (peak 1) is approximated by

$$\theta_1 = \alpha \lambda^2 N (r_2/d_2)^{1/2}. \tag{8}$$

From a large number of simulation experiments for a typical focus plasma, α turned out to be a numerical constant:

$$\alpha = 6.9 \times 10^{-14} \text{ cm} \tag{9}$$

if λ is given in cm, N in cm^{-3}, and θ in rad.

The rays which cause peak 2 enter the plasma but do not penetrate to the inner gradient region. They are deflected twice as shown in Fig. 5 so that the angle corresponding to peak 2 can be given by

$$\theta_2 = 2b/R\{(1 + f/2)(1 - b^2/R^2)^{1/2} - [1 - b^2/R^2(1 + f)]^{1/2}\}, \tag{10}$$

if $f = 1 - n^2 \ll 1$. In cases where the condition

$$f \ll \frac{R^2}{b^2} - 1 \tag{11}$$

holds, Eq. (10) reduces to the simple form

$$\theta_2 = \frac{b \cdot f}{(R^2 - b^2)^{1/2}}. \tag{12}$$

With Eqs. (5) and (7) and substituting R and b with the plasma parameters $R = r_2$ and $b = 1/2(r_1 + r_2)$, Eq. (12) becomes

$$\theta_2 = A \frac{\lambda^2 N (r_1 + r_2)}{(3r_2^2 - 2r_1 r_2 - r_1^2)^{1/2}}. \tag{13}$$

It should be noted that θ_2 depends on maximum density

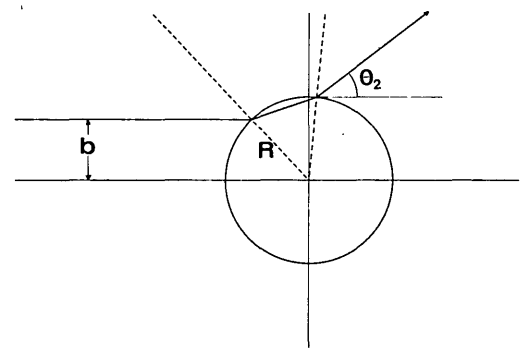

Fig. 5. Ray deflection in a plasma cylinder of constant density.

and dimensions of the plasma but not on dimensions of the gradient regions d_1 and d_2. The intensity of peak 2 is proportional to the plateau width of the density profile which may change, especially at the end of compression.

Since the rays causing peak 3 are influenced by both the outer and inner gradient regions, Eqs. (8) and (12) have to be combined. Using Eq. (5) and considering $b \simeq r_1$ the angle corresponding to peak 3 is expressed by

$$\theta_3 = A \frac{\lambda^2 N r_1}{(r_2^2 - r_1^2)^{1/2}} - \alpha \lambda^2 (N - N_0 \ldots) \left(\frac{r_1}{d_1}\right)^{1/2}. \tag{14}$$

Equation (14) holds if the width of the plateau $\delta - 2(d_1 + d_2)$ is smaller than $4(d_1 + d_2)$.

The central maximum stems from undeflected or slightly deflected rays near the cylinder axis or outer regions and therefore is asymmetric with respect to the center.

III. Schlieren Optics

Angular ray distributions can be transformed into intensity distributions on the film plane by either the bright-field or the dark-field schlieren method.

Since the marked peaks of the angular distribution (which have almost negligible intensity compared with the central maximum) are of primary interest, the dark-field schlieren method is used. A beam stop of radius ρ in the focal plane of the schlieren lens eliminates all rays in the interval

$$-\theta^* < \theta < \theta^*, \tag{15}$$

$$\theta^* = \arctan \rho / f_1, \tag{16}$$

where f_1 denotes the focal length of the schlieren lens (Fig. 6).

The beam stop radius ρ determines whether a schlieren picture occurs and what part of the angular ray distribution plotted in Fig. 4 contributes to it. If

$$|\theta_3| < \theta^* < \theta_1, \tag{17}$$

only the rays deflected by the outer gradient of the density profile (peak 1 in Fig. 4) pass by the beam stop. Peak 2, stemming from an eventually existing plateau, can cause a modulation of the intensity distribution. But if

$$\theta^* < |\theta_3|, \tag{18}$$

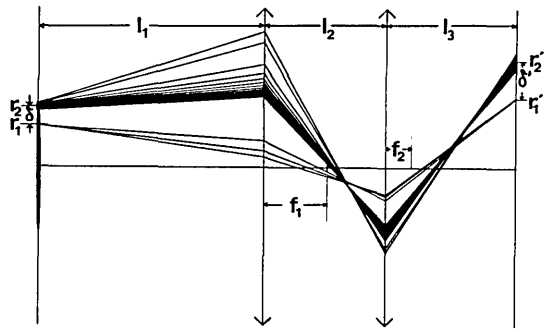

Fig. 6. Ray traces through the schlieren system: $N = 2 \times 10^{18}$ cm^{-3}, $N_0 = 10^{17}$ cm^{-3}, $r_1 = 9.75$ mm, $r_2 = 10.25$ mm, $d_1 = d_2 = 0.05$ mm, $\lambda = 600$ nm, $l_1 = 177$ cm, $l_2 = 96$ cm, $l_3 = 102$ cm, $f_1 = 50$ cm, $f_2 = 20$ cm, $\rho = 0.75$ mm.

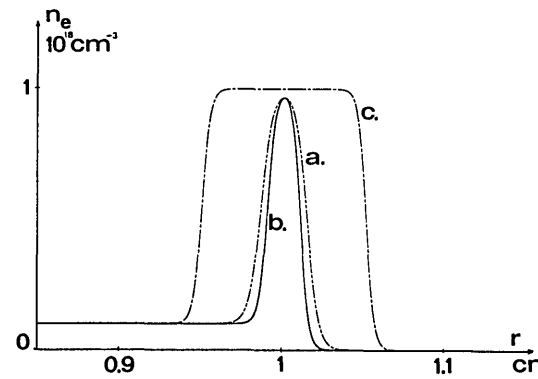

Fig. 7. Typical examples of density profiles: (a) $N = 10^{18}$ cm^{-3}, $N_0 = 10^{17}$ cm^{-3}, $r_1 = 9.86$ mm, $r_2 = 10.14$ mm, $d_1 = d_2 = 0.07$ mm; (b) $N = 10^{18}$ cm^{-3}, $N_0 = 10^{17}$ cm^{-3}, $r_1 = 9.9$ mm, $r_2 = 10.1$ mm, $d_1 = d_2 = 0.05$ mm; (c) $N = 2.10^{18}$ cm^{-3}, $N_0 = 10^{17}$ cm^{-3}, $r_1 = 9.5$ mm, $r_2 = 10.5$ mm, $d_1 = d_2 = 0.05$ mm.

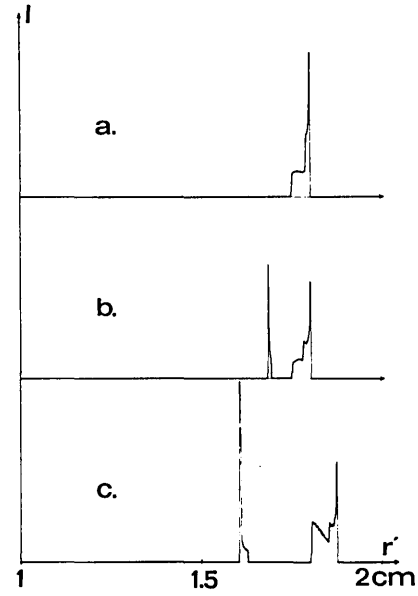

Fig. 8. Intensity distributions on the detector plane for the three typical profiles plotted in Fig. 7.

the rays deflected at the inner gradient (peak 3) also contribute to the intensity distribution. For this case ray traces through a special schlieren system (see Sec. V) are plotted in Fig. 6 (note the different horizontal and vertical scales; stopped rays are not plotted).

Intensity distributions on the detector plane were studied for various density profiles. Three typical profiles are plotted in Fig. 7. Profiles *a* and *b* differ only in gradients, whereas profile *c* has a plateau. The corresponding intensity distributions are plotted in Fig. 8. In the case of profile *a*, condition (17) is satisfied; therefore only one peak appears, which corresponds to peak 1 of Fig. 4. Rays corresponding to peak 3 in Fig. 4 are stopped and peak 2 does not appear because of the absence of a plateau in profile *a*. In the case of profile *b*, condition (18) is satisfied and two peaks appear in the corresponding intensity distribution Fig. 8(b). If the profile has a plateau region and the density is great enough to satisfy condition $\theta_2 > \theta^*$, the outer peak becomes much wider than the inner one [Fig. 8(c)].

Note that existence, radial position, intensity, and width of the peaks in the detector plane (see Fig. 8) are very sensitive to variations of density, density gradients, and width of the density profile (see Fig. 7). This opens the possibility of getting ranges of the plasma parameters by simply considering the measuring range of the schlieren system and by comparing simulated schlieren pictures with ones taken experimentally.[8] For this purpose the radial position of the intensity pattern on the detector plane is calculated in transforming the object r into the image r' using geometrical optics and the data of the schlieren system of Fig. 6.

Since the lateral dimensions of the object and the image are much smaller than the longitudinal ones of the optical system, the image is given by

$$r' = Qr + P \tan\theta, \tag{19}$$

where Q and P are constants of the schlieren system of Fig. 6. Without spherical aberrations and with a well-defined object plane $P = 0$; Q denotes the lateral magnification.

Equation (1) is a necessary condition for the applicability of geometrical optics but not a sufficient one in cases where diffraction must be considered because of small-scale phenomena as the gradient regions of the density profile of Figs. 1 and 7. The effect of interaction of diffracted and refracted light, which causes degradation of the schlieren picture, has to be negligible if one is to resolve the peaked intensity distributions on the film. In our case diffraction can be neglected if the dimensions of the gradient regions are larger than a critical value

$$d_{1,2} > k \frac{\lambda}{\theta^*}, \tag{20}$$

where the numerical factor has been theoretically estimated, $k = 1/16$, and experimentally checked. The inequalities of the previous sections can be used if condition (20) is satisfied. The given angles refer to the maxima of the intensity pattern.

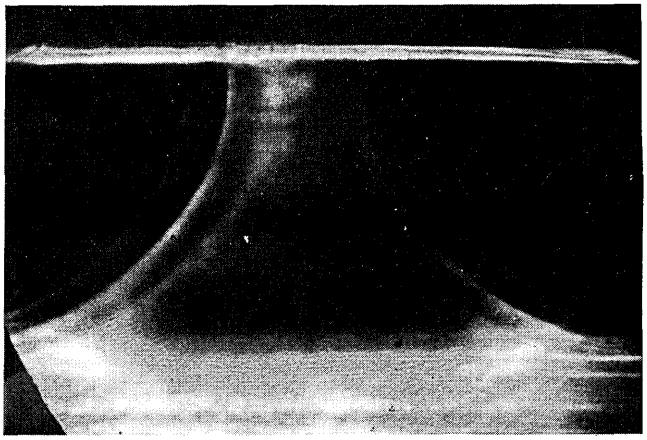

Fig. 9. Schlieren pictures of the SPEED 1 pinch plasma.

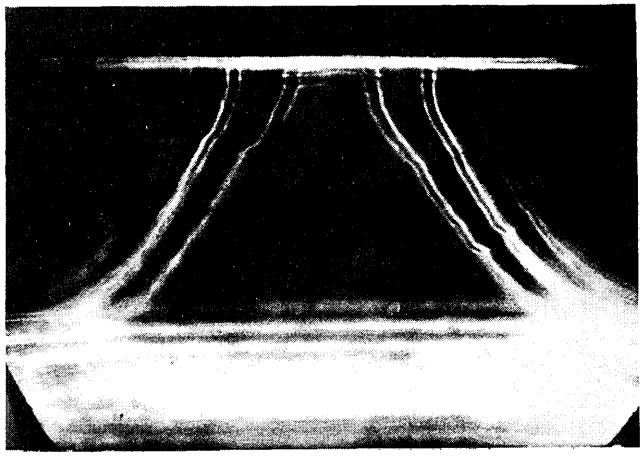

Fig. 10. Schlieren picture of the SPEED 1 pinch plasma.

IV. Parameter Ranges

Single peaked intensity distributions [Fig. 8(a)] stem from the outer gradient region of the plasma. Combining Eqs. (8) and (17) results in

$$N\left(\frac{r_2}{d_2}\right)^{1/2} > \frac{\theta^*}{\alpha\lambda^2}. \tag{21}$$

Setting $r = r_2$ in Eq. (19),

$$r_2' = Qr_2 + P\alpha\lambda^2 N\left(\frac{r_2}{d_2}\right)^{1/2} \tag{22}$$

gives the necessary second equation to estimate the range of the parameters r_2 and $N(d_2)^{-1/2}$, but N and d_2 cannot be separately determined in this case.

Double peaked intensity distributions [Fig. 8(b)], however, allow not only using Eq. (21) (outer peak) but also the combination of Eqs. (14) and (18):

$$(N - N_0)\left(\frac{r_1}{d_1}\right)^{1/2} - \frac{A}{\alpha}\frac{Nr_1}{(r_2^2 - r_1^2)^{1/2}} > \frac{\theta^*}{\alpha\lambda^2} \tag{23}$$

(inner peak).

Inserting r_2 and r_1 into Eq. (19) and taking the difference of the two equations gives the thickness of the plasma layer, and with Eqs. (8) and (14)

$$\delta = \frac{\delta'}{Q} - \frac{P\alpha\lambda^2}{Q}\left[(N - N_0)\left(\frac{r_1}{d_1}\right)^{1/2} + N\left(\frac{r_2}{d_2}\right)^{1/2} - \frac{A}{\alpha}\frac{Nr_1}{(r_2^2 - r_1^2)^{1/2}}\right], \tag{24}$$

with $\delta' = r_2' - r_1'$ denoting the distance of the peaks of the intensity distribution, as shown in Fig. 6.

Equations (21), (23), and (24) give the upper limit of the thickness

$$\delta < \frac{\delta' - 2P\theta^*}{Q}; \tag{25}$$

the lower limit results from Eq. (20),

$$\delta = 4d_{1,2} > \frac{\lambda}{4\theta^*}. \tag{26}$$

Combining Eqs. (21), (23), and (24) with $\delta > 0$ gives

$$\frac{2\theta^*}{\alpha\lambda^2} < (N - N_0)\left(\frac{r_1}{d_1}\right)^{1/2} + N\left(\frac{r_2}{d_2}\right)^{1/2} - \frac{A}{\alpha}\frac{Nr_1}{(r_2^2 - r_1^2)^{1/2}} < \frac{\delta'}{P\alpha\lambda^2}. \tag{27}$$

With the realistic assumptions for a plasma layer $N \gg N_0$ and $\delta \ll 1/2(r + r_2)$, assuming $d_1 = d_2$ as in Eq. (26) approximately $\frac{1}{4}\,\delta$ (profiles without plateau, e.g., a and b of Fig. 7), and developing Eq. (27) in series of $\delta(r_1 + r_2)^{-1}$, the range of the plasma density is

$$\frac{\theta^*}{\alpha\lambda^2\gamma}\left(\frac{\delta}{R}\right)^{1/2} < N < \frac{\delta'}{2P\alpha\lambda^2\gamma}\left(\frac{\delta}{R}\right)^{1/2}, \tag{28}$$

with $R = \frac{1}{2}\,(r_1 + r_2)$ denoting the mean radius of the cylindrical plasma layer and $\gamma = 1.54$.

Hence, knowing the peak separation of the intensity distribution and the parameters of the schlieren system, the parameter ranges of both density N and thickness of the plasma layer δ are accessible.

V. Application to SPEED 1

Dark-field schlieren pictures of the SPEED 1 pinch plasma were taken using a mode-locked dye laser and a pulsed image converter. The optical setup is schematically shown in Fig. 6. This technique resulted in framing sequences of two or three 5-nsec time-delayed schlieren pictures, superimposed on the film, with time resolution below 100 psec. Two examples are given in Figs. 9 and 10. It should be noted that instead of the r, plane used in the schematic drawings of Figs. 2, 3, and 6 the r,z plane is imaged (z axis denoting the focus axis).

The intensity pattern of interest is the curved section symmetric to the focus axis, which stems mainly from radial electron density gradients of the rapidly compressed plasma sheath. These curved sections consist of one (see Fig. 9) or two separate lines (see Fig. 10). From a lot of these pictures the following is observed:

(i) Double structured intensity patterns are correlated to focus discharges with high neutron production.

(ii) Width and intensity of the two lines are similar, the distance between them is independent of the radial position of the plasma layer.

(iii) The distance does not change during plasma compression and is in the interval $\delta' = 1.2$–1.4 mm.

From these observations parameter ranges for density, density gradients, and thickness of the plasma layer can be derived.

Since the width and intensities of the two lines are similar, a plateau region is not very likely to exist in the density profile [see Fig. 7(c)]. The approximation formulas given in the previous section can be applied. Using the experimental data ($\lambda = 6 \times 10^{-7}$ m, $\theta^* = 1.5$ m rad, $Q = 1.7$, $P = 15$ cm, $\delta' = 1.2$ mm) the ranges for the plasma parameters turn out as follows:

thickness of the plasma layer: $0.1 \text{ mm} < \delta \leq 0.4 \text{ mm}$;

density: $4 \times 10^{18} \left(\frac{\delta}{R}\right)^{1/2} \text{cm}^{-3} < N < 10^{19} \left(\frac{\delta}{R}\right)^{1/2} \text{cm}^{-3}$;

density gradient: $\frac{1.6 \times 10^{19}}{(R\delta)^{1/2}} \text{cm}^{-4} < \frac{N}{d_2} \leq \frac{4 \times 10^{19}}{(R \cdot \delta)^{1/2}} \text{cm}^{-4}$.

These ranges can be further narrowed by successive simulation experiments with systematic parameter variations. This has been done for different radial positions of the plasma layer.[8]

VI. Summary

Computer simulations proved to be a useful tool for interpretation and quantitative evaluation of schlieren pictures taken from fast varying plasmas with axial symmetry.

The simulation experiments revealed that not the plasma itself but an extended caustics is the object imaged by the schlieren system and that the angular distribution of the rays deflected by the plasma layer is unexpectedly structurized. From these angular distributions the influencing plasma parameters have been identified. Taking the measuring range of the optical system into consideration the ranges of the plasma parameters are accessible.

This simulation method has been used to evaluate schlieren pictures of the extremely thin and fast varying plasma layer of the high voltage plasma focus SPEED 1. The plasma parameters density and thickness of the layer have been given.

References

1. H. Maecker, "Elektroneudichte und Temperatur in der Säuledes Hochstrom-kohlebogens," Z. Phys. **136**, 119 (1953).
2. T. P. Davies, "Schlieren Photography—Short Bibliography and Review," Opt. Laser Technol. **13**, 37 (1981).
3. R. Haas, H. Krompholz, L. Michel, F. Ruhl, K. Schonbach, and G. Herziger, "Regular Density Structures in the Plasma Focus," Phys. Lett. A **88**, 403 (1982).
4. F. Keilmann, "An Infrared Schlieren Interferometer for Measuring Electron Density Profiles," Plasma Phys. **14**, 111 (1972).
5. H. Schmidt and B. Rueckle, "Beam Deviation Method as a Diagnostic Tool for the Plasma Focus," Appl. Opt. **17**, 1275 (1978).
6. U. Kogelschatz and W. R. Schneider, "Quantitative Schlieren Techniques Applied to High Current Arc Investigations," Appl. Opt. **11**, 1822 (1972).
7. G. Decker, W. Kies, and G. Pross, "The First and the Final Fifty Nanoseconds of a Fast Focus Discharge," Phys. Fluids **26**, 571 (1983).
8. G. Decker, R. Deutsch, W. Kies, and J. Rybach, "Plasma Layers of Fast Focus Discharges—Schlieren Pictures Experimentally Taken and Computer Simulated," Plasma Phys. accepted for publication (Jan. 1985).